Theory of resonantly enhanced near-field imaging

Mankei Tsang[1] **and Demetri Psaltis**[1,2]

[1]*Department of Electrical Engineering, California Institute of Technology, Pasadena, California 91125, USA*

[2]*Institute of Imaging and Applied Optics, Ecole Polytechnique Fédérale de Lausanne, CH-1015 Lausanne, Switzerland*
mankei@optics.caltech.edu

Abstract: We investigate the fundamental issues of power transfer and far-field retrieval of subwavelength information in resonantly enhanced near-field imaging systems. It is found that high-quality resonance of the imaging system, such as that provided by dielectric resonators, can drastically enhance the power transfer from the object to the detector or the working distance. The optimal power transfer condition is shown to be the same as the critical coupling condition for resonators. The combination of a dielectric planar resonator with a solid immersion lens is proposed to project resonantly enhanced near-field spatial frequency components into the far field with the same resolution limit as that for solid immersion microscopy, but with much improved signal power throughput or working distance for resonant spatial frequencies.

References and links

1. E. Betzig and J. K. Trautman, "Near-field optics: Microscopy, spectroscopy, and surface modification beyond the diffraction limit," Science **257**, 189-195 (1992).
2. J. B. Pendry, "Negative refraction makes a perfect lens," Phys. Rev. Lett. **85**, 3966-3969 (2000).
3. V. G. Veselago, "Electrodynamics of substances with simultaneously negative values of ε and μ," Sov. Phys. Usp. **10**, 509-514 (1968).
4. N. Garcia and M. Nieto-Vesperinas, "Left-handed materials do not make a perfect lens," Phys. Rev. Lett. **88**, 207403 (2002).
5. D. R. Smith, D. Schurig, M. Rosenbluth, S. Schultz, S. A. Ramakrishna, and J. B. Pendry, "Limitations on subdiffraction imaging with a negative refractive index slab," Appl. Phys. Lett. **82**, 1506-1508 (2003).
6. K. J. Webb, M. Yang, D. W. Ward, and K. A. Nelson, "Metrics for negative-refractive-index materials," Phys. Rev. E **70**, 035602(R) (2004).
7. M. I. Stockman, "Criterion for negative refraction with low optical losses from a fundamental principle of causality," Phys. Rev. Lett. **98**, 177404 (2007).
8. N. Fang, H. Lee, C. Sun, and X. Zhang, "Sub-diffraction-limited optical imaging with a silver superlens," Science **308**, 534-537 (2005).
9. D. O. S. Melville and R. J. Blaikie, "Super-resolution imaging through a planar silver layer," Opt. Express **13**, 2127-2134 (2005).
10. C. Luo, S. G. Johnson, J. D. Joannopoulos, and J. B. Pendry, "All-angle negative refraction without negative effective index," Phys. Rev. B **65**, 201104 (2002).
11. C. Luo, S. G. Johnson, J. D. Joannopoulos, and J. B. Pendry, "Subwavelength imaging in photonic crystals," Phys. Rev. B **68**, 045115 (2003).

12. M. Tsang and D. Psaltis, "Reflectionless evanescent wave amplification via two dielectric planar waveguides," Opt. Lett. **31**, 2741-2743 (2006).
13. M. Tsang and D. Psaltis, "Reflectionless evanescent wave amplification via two dielectric planar waveguides: erratum," Opt. Lett. **32**, 86 (2007).
14. R. B. Adler, L. J. Chu, and R. M. Fano, *Electromagnetic Energy Transmission and Radiation* (Wiley, New York, 1960).
15. A. Yariv, "Universal relations for coupling of optical power between microresonators and dielectric waveguides," Electron. Lett. **36**, 321 (2000).
16. M. Cai, O. Painter, and K. J. Vahala, "Observation of critical coupling in a fiber taper to a silica-microsphere whispering-gallery mode system," Phys. Rev. Lett. **85**, 74-77 (2000).
17. S. M. Mansfield and G. S. Kino, "Solid immersion microscope," Appl. Phys. Lett. **57**, 2615-2616 (1990).
18. B. D. Terris, H. J. Mamin, D. Rugar, W. R. Studenmund, and G. S. Kino, "near-field optical data storage using a solid immersion lens," Appl. Phys. Lett. **65**, 388-390 (1994).
19. L. P. Ghislain, V. B. Elings, K. B. Crozier, S. R. Manalis, S. C. Minne, K. Wilder, G. S. Kino, and C. F. Quate, "Near-field photolithography with a solid immersion lens," Appl. Phys. Lett. **74**, 501-503 (1999).
20. I. I. Smolyaninov, J. Elliot, A. V. Zayats, and C. C. Davis, "Far-field optical microscopy with a nanometer-scale resolution based on the in-plane image magnification by surface plasmon polaritons," Phys. Rev. Lett. **94**, 057401 (2005).
21. I. I. Smolyaninov, C. C. Davis, J. Elliot, G. A. Wurtz, and A. V. Zayats, "Super-resolution optical microscopy based on photonic crystal materials," Phys. Rev. B **72**, 085442 (2005).
22. A. Salandrino and N. Engheta, "Far-field subdiffraction optical microscopy using metamaterial crystals: theory and simulations," Phys. Rev. B **74**, 075103 (2006).
23. Z. Jacob, L. V. Alekseyev, and E. Narimanov, "Optical Hyperlens: Far-field imaging beyond the diffraction limit," Opt. Express **14**, 8247-8256 (2006).
24. Z. Liu, H. Lee, Y. Xiong, C. Sun, and X. Zhang, "Far-field optical hyperlens magnifying sub-diffraction-limited objects," Science **315**, 1686 (2007).
25. I. I. Smolyaninov, Y.-J. Hung, and C. C. Davis, "Magnifying superlens in the visible frequency range," Science **315**, 1699-1701 (2007).
26. J. D. Jackson, *Classical Electrodynamics* (Wiley, New York, 1989).
27. D. F. Edwards and E. Ochoa, "Infrared refractive index of diamond," J. Opt. Soc. Am. **71**, 607-608 (1981), and references therein.
28. C. D. Clark, P. J. Dean, and P. V. Harris, "Intrinsic edge absorption in diamond," Proc. R. Soc. London, Ser. A **277**, 312-329 (1964).
29. S. A. Ramakrishna and J. B. Pendry, "Removal of absorption and increase in resolution in a near-field lens via optical gain," Phys. Rev. B **67**, 201101(R) (2003).
30. M. P. Nezhad, K. Tetz, and Y. Fainman, "Gain assisted propagation of surface plasmon polaritons on planar metallic waveguides," Opt. Express **12**, 4072-4079 (2004).
31. A. Yariv, *Quantum Electronics* (Wiley, New York, 2001).
32. M. Shinoda *et al.*, "High-density near-field readout using diamond solid immersion lens," Jpn. J. Appl. Phys. **45**, 1311-1313 (2006).
33. E. J. Candès, J. Romberg, and T. Tao, "Robust uncertainty principles: exact signal reconstruction from highly incomplete frequency information," IEEE Trans. Inf. Theory **52**, 489-509 (2006).
34. S. H. Zaidi and S. R. J. Brueck, "Multiple-exposure interferometric lithography," J. Vac. Sci. Technol. B **11**, 658-666 (1993).
35. S. Ruschin and A. Leizer, "Evanescent Bessel beams," J. Opt. Soc. Am. A **15**, 1139-1143 (1998).
36. J. D. Joannopoulos, R. D. Meade, J. N. Winn, *Photonic Crystals* (Princeton Univ. Press, Princeton, NJ, 1995).
37. P. J. Reece, V. Garcés-Chávez, and K. Dholakia, "Near-field optical micromanipulation with cavity enhanced evanescent waves," Appl. Phys. Lett. **88**, 221116 (2006).
38. A. Karalis, J. D. Joannopoulos, and M. Soljačić, "Efficient wireless non-radiative mid-range energy transfer," e-print arXiv:physics/0611063v2 (Ann. Phys., in press).
39. A. Kurs, A. Karalis, R. Moffatt, J. D. Joannopoulos, P. Fisher, and M. Soljačić, "Wireless power transfer via strongly coupled magnetic resonances," Science **317**, 83-86 (2007).
40. A. N. Boto, P. Kok, D. S. Abrams, S. L. Braunstein, C. P. Williams, and J. P. Dowling, "Quantum interferometric optical lithography: exploiting entanglement to beat the diffraction limit," Phys. Rev. Lett. **85**, 2733-2736 (2000).
41. M. Tsang, "Relationship between resolution enhancement and multiphoton absorption rate in quantum lithography," Phys. Rev. A **75**, 043813 (2007).
42. D. Psaltis, S. R. Quake, and C. Yang, "Developing optofluidic technology through the fusion of microfluidics and optics," Nature (London) **442**, 381-386 (2006).
43. Q. Wu, G. D. Feke, R. D. Grober, and L. P. Ghislain, "Realization of numerical aperture 2.0 using a gallium phosphide solid immersion lens," Appl. Phys. Lett. **75**, 4064-4066 (1999).
44. M. Shinoda, K. Saito, T. Kondo, M. Furuki, M. Takeda, A. Nakaoki, M. Sasaura, and K. Fujiura, "High-density near-field readout using solid immersion lens made of $KTaO_3$ monocrystal," Jpn. J. Appl. Phys. **45**, 1332-1335

(2006).

45. M. O. Scully, "Enhancement of the index of refraction via quantum coherence," Phys. Rev. Lett. **67**, 1855-1858 (1991).

46. V. Anant, M. Rådmark, A. F. Abouraddy, T. C. Killian, and K. K. Berggren, "Pumped quantum systems: Immersion fluids of the future?" J. Vac. Sci. Technol. B **23**, 2662-2667 (2005).

1. Introduction

Detecting evanescent waves is one of the most important and challenging problems in imaging. Near-field scanning optical microscopy (NSOM) has had considerable success [1] but requires scanning and a probe in close proximity to the object. Both requirements are undesirable for certain imaging applications, such as optical lithography. A proposal by Pendry [2] that a negative-refractive-index slab [3] amplifies evanescent waves promises to solve both problems, although the evanescent-wave amplification is severely limited by loss [4, 5, 6], while negative-index materials are necessarily quite lossy due to practical and fundamental issues [7]. On the other hand, impressive experiments by Fang *et al.* [8] and Melville and Blaikie [9] have demonstrated the use of surface-plasmon polaritons (SPP) for resonantly enhanced near-field imaging [2]. The presence of a thin dielectric spacer layer between the silver slab and the object in each demonstration, however, means that the problem of close contact has not yet been overcome.

Another interesting route to non-contact and scanning-free subwavelength imaging is by the use of a photonic crystal slab [10, 11]. A photonic crystal is able to focus propagating waves [10] and amplify evanescent waves via coupling to the bound states [11]. As the bound states of a photonic crystal have much lower loss than SPP on metal surfaces, a photonic crystal slab can be placed farther away from the object and still produces significant evanescent-wave enhancement. That said, in practice it is still a major challenge to fabricate three-dimensional photonic crystals for two-dimensional imaging.

To improve upon existing near-field imaging techniques, we have proposed a simple idea: the use of dielectric planar waveguides for near-field imaging [12, 13], where evanescent waves can be amplified by coupling to the waveguide modes. Although the resolution is still limited by the refractive index much like photonic crystals, the extremely low loss and fabrication simplicity potentially allows dielectric planar waveguides to complement or surpass previous techniques.

In this paper, we investigate the fundamental issues of power transfer and retrieval of near-field information in near-field imaging systems. In Section 2, we show how the signal power throughput and the working distance can be maximized using high-quality resonance, such as that provided by dielectric resonators. Previous studies have addressed the condition of evanescent growth in metamaterials due to loss [4, 5, 6], but here we focus on arguably more important metrics for near-field imaging systems in general, namely the signal power throughput and the working distance, since the ultimate goal of evanescent-wave amplification is to increase the signal-to-noise ratio and enable remote detection of near-field information. We find that the efficiency of power transfer from the source to the detector depends crucially on the evanescent-wave reflection coefficient of the imaging system. In our previous studies [12, 13], we have already argued for the importance of this coefficient. Here we substantiate this argument and derive the ideal conditions on the coefficient and other system parameters in which power is optimally transferred.

For a realistic near-field source, the optimal power transfer condition is identical to the critical coupling condition for resonators [14, 15, 16]; in fact, any near-field imaging device based on the principle of evanescent-wave amplification can be regarded as a resonator. As is well known for resonators, low loss allows a resonant imaging device to be placed farther away from the source while still maintaining an appreciable detected signal. This correspondence between resonators and near-field imaging systems thus demonstrates the advantage of low-

loss dielectric resonators.

In order to illustrate the use of high-quality resonance for near-field imaging in practice, in Section 3, we propose the method of resonantly enhanced solid immersion microscopy (RESIM), where a dielectric planar resonator is combined with a solid immersion lens [17] for far-field observation of resonantly enhanced evanescent waves. A solid immersion lens is a high-refractive-index plano-convex lens that converts the near field in the immediate vicinity of the planar surface to propagating waves, which are then focused in free space by the convex surface, achieving an effective numerical aperture up to the refractive index of the lens [17]. This technique has been proposed and demonstrated for microscopy [17], optical data storage [18], and lithography applications [19], but the working distance and the resolution are severely limited by the exponential decay of evanescent waves in free space. With the addition of a dielectric slab, we show that the transmission of resonant spatial frequency components can be enhanced by orders of magnitude, such that weaker signals can be detected above the noise floor of the detector, the working distance can be increased, and the signal-to-noise ratio can be improved. The use of dielectric-metallic structures for microscopy has also been proposed and demonstrated in impressive experiments recently [20, 21, 22, 23, 24, 25], but again due to the relatively high loss of metals, the object must be extremely close to the imaging device.

2. Power transfer in near-field imaging systems

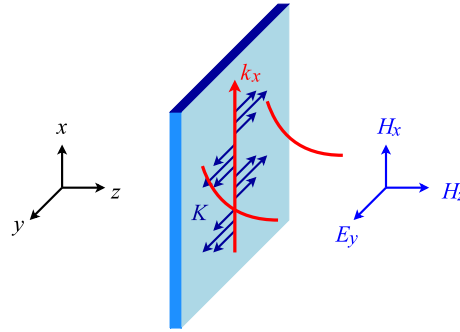### 2.1. Ideal near-field current source

Fig. 1. An ideal near-field surface current source that produces a TE evanescent wave.

To address the issue of energy conservation and power transfer in evanescent-wave scattering, we first assume that an incident evanescent wave is produced in free space by an ideal surface current source. For TE evanescent waves, let the harmonic current at frequency ω be

$$\mathbf{J}(\mathbf{x}) = \hat{\mathbf{y}} K \delta(z) \exp(ik_x x), \tag{1}$$

where $k_x > k \equiv \omega/c = 2\pi/\lambda$, as depicted in Fig. 1. In the following we shall focus on the TE waves. Analysis of TM waves follows similar arguments by assuming an x-polarized $\mathbf{J}$ and a charge distribution ρ that satisfy the continuity equation.

By solving the Maxwell's equations, the resultant TE evanescent wave for $z \geq 0$ can be expressed as

$$\mathbf{E}_i(\mathbf{x}) = \hat{\mathbf{y}} \frac{iK\mu_0\omega}{2\kappa} \exp(-\kappa z + ik_x x), \tag{2}$$

$$\mathbf{H}_i(\mathbf{x}) = \frac{K}{2}\left(\hat{\mathbf{x}} + \hat{\mathbf{z}}\frac{ik_x}{\kappa}\right) \exp(-\kappa z + ik_x x), \tag{3}$$

where $\kappa \equiv \sqrt{k^2 - k_x^2}$ is the decay constant. The average power supplied by the current source is equal to the negative rate of work done by the field at the current source, and is given by [26]

$$P = -\frac{1}{2} \int d^3x \, \mathrm{Re}\{\mathbf{J}^* \cdot \mathbf{E}\}. \tag{4}$$

Since the current and the created electric field are $\pi/2$ out of phase, the power supplied by the current source to sustain the evanescent wave is zero, as expected.
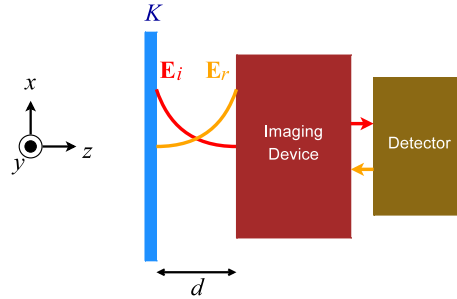

Fig. 2. A near-field imaging device together with a detector located at a working distance d away from the current source.

Now consider a near-field imaging device together with a detector located at $z \geq d$, as shown in Fig. 2. The imaging device can be an NSOM tip, a negative-index slab, a silver thin film, a photonic crystal, a dielectric slab, or any dielectric-metallic structure, while the detector can be any energy sink that extracts power and thus information from the device, such as a charge-coupled device array, a photoresist, or a solid immersion lens that converts the near field into far-field radiation [17]. The specific details of the system need not concern us for now, but assume that it produces a reflected evanescent wave of the form

$$\mathbf{E}_r(z=d) = \Gamma \mathbf{E}_i(z=d), \tag{5}$$

$$\mathbf{E}_r(z=0) = \hat{\mathbf{y}} \frac{i\Gamma K \mu_0 \omega}{2\kappa} \exp(-2\kappa d) \exp(ik_x x), \tag{6}$$

where Γ is the evanescent-wave reflection coefficient from the system. According to Eq. (4), the power per unit area supplied by the current source then becomes

$$\frac{P}{A} = \frac{|K|^2 \mu_0 \omega}{4\kappa} \mathrm{Im}\{\Gamma\} \exp(-2\kappa d), \tag{7}$$

where $\mathrm{Im}\{\Gamma\}$ is the imaginary part of Γ. Any power supplied by the source must be accompanied by a non-zero Poynting vector in the z direction in free space [26]:

$$S_z(0 < z < d) = \frac{1}{2} \mathrm{Re}\{\mathbf{E} \times \mathbf{H}^*\} \cdot \hat{\mathbf{z}} \equiv \frac{P}{A}. \tag{8}$$

The tunneling Poynting vector results from the interference of the incident evanescent wave $\mathbf{E}_i$ and the reflected wave $\mathbf{E}_r$, even though the Poynting vector of each evanescent wave in the z direction is zero individually. By energy conservation, the supplied power must all be consumed by the system. Hence the imaginary part of the reflection coefficient, $\mathrm{Im}\{\Gamma\}$, plays the role of system resistance, which must account for all useful power extracted by the detector, as well as any unwanted dissipation in the device, such as absorption and scattering loss. For example, the

total power extracted by an NSOM probe is consumed mostly by the scattering of the near field into far-field radiation, and only a small portion of the total power can be coupled into the fiber mode and reach the detector. Similarly, Γ may be regarded as the complex system impedance.

In general, the imaging system can be spatially inhomogeneous and produces an arbitrary evanescent-wave scattering pattern. $\text{Im}\{\Gamma\}$ can then be regarded as the inner product of the scattering pattern with the current distribution, as defined by Eq. (4). Hence any system that extracts power from the evanescent wave must produce a reflected wave of the form given by Eq. (6), with a non-zero $\text{Im}\{\Gamma\}$, to "tell" the source to give up power. The analysis can also be generalized to an arbitrary current source distribution and an arbitrary photonic structure, as shown in Appendix A. In that case, it is necessary to express the waves in a more appropriate basis than plane waves and use Mie scattering theory, but the analysis of the planar geometry here already captures most of the essential physics.

There is no fundamental restriction on the magnitude of $\text{Im}\{\Gamma\}$, other than the fact that a passive system must have a non-negative $\text{Im}\{\Gamma\}$. When the evanescent wave is coupled to a resonance mode of the device, such as the SPP on a metal surface or a dielectric waveguide mode, the magnitude of Γ can be resonantly enhanced beyond unity and approach infinity [2, 12] depending on the quality of the resonance, so that the evanescent wave can appear to be growing even in free space for $0 < z < d$. As is generic for any kind of resonance, resonance can be defined as the condition at which the system becomes purely dissipative, or equivalently when the system impedance Γ is purely imaginary. In other words, resonance is always desirable for obtaining the maximum $\text{Im}\{\Gamma\}$ and the highest power transfer. Ideally the imaging device should have negligible dissipation compared with the detector, so that the detector consumes most power.

We have argued in previous studies [12, 13] that it is desirable for an unloaded imaging device to have zero evanescent-wave reflection and unit evanescent-wave transmission. Under such a condition, the imaging device plays the role of a "circuit wire" that transmits the evanescent wave to the detector. It is an ideal condition if the detector itself is a purely dissipative load in response to the evanescent wave, but in general, the imaging device should provide impedance matching with respect to the complex response of the detector and maximize the power transfer to the detector by maximizing the loaded $\text{Im}\{\Gamma\}$.

Equation (7) also shows that the total consumed power decays exponentially with respect to the working distance d, suggesting that the loaded $\text{Im}\{\Gamma\}$ should have an extremely large magnitude to compensate for the exponential decay. Furthermore, the higher the spatial frequency k_x, the larger the value of κ, so the magnitude of $\text{Im}\{\Gamma\}$ must be even larger to obtain higher resolution. It is well known that the amplitude response at resonance is proportional to the quality factor Q of the resonance mode. The maximum $\text{Im}\{\Gamma\}$ is then proportional to the Q of the resonance mode, and a high Q is thus crucial for maximizing the power transfer and the working distance.

To estimate the magnitude of $\text{Im}\{\Gamma\}$ relative to Q, recall that the definition of Q is ω times the energy stored in a resonator mode divided by the dissipated power. The dissipated power per unit area is given by Eq. (7) and proportional to $\text{Im}\{\Gamma\}$, but the energy stored per unit area cannot be derived from Γ at resonance alone. It is still possible to obtain a lower bound for the energy, as the stored energy must at least be larger than the energy stored in the reflected evanescent tail, which is proportional to $|\Gamma|^2$ and to $\text{Im}\{\Gamma\}^2$ at resonance. It can be shown after some algebra that

$$\text{Im}\{\Gamma\}_{\text{resonance}} \leq 4\left(1 - \frac{k^2}{k_x^2}\right)Q < 4Q. \tag{9}$$

For example, assuming a diamond thin film with a thickness of 20 nm, a complex refractive index $n = 2.7[1 + i/(2Q_i)]$ at $\lambda = 230$ nm [27], and a material Q_i of 10^5 [28], a TE mode exists

at the spatial frequency of $k_x = 1.7k$ with a resonant unloaded $\text{Im}\{\Gamma\}$ of 5.3×10^4. A thickness of 40 nm produces a TE mode at $k_x = 2.2k$ with a resonant $\text{Im}\{\Gamma\}$ of 2.5×10^4. If the slab is loaded by, say, a photoresist next to it, then the loaded $\text{Im}\{\Gamma\}$ must decrease. The unloaded values calculated above represent the maximum resonant enhancement that can be obtained.

While the upper bound given by Eq. (9) is not tight, it already places a severe constraint on the resonant enhancement for SPP systems, as the maximum Q for SPP in the visible spectrum is only on the order of 10 in practice.

As is well known, Q can be enhanced by introducing gain to compensate for loss. This has been proposed for SPP [29, 30], but the high gain required for SPP is relatively difficult to achieve and adds a large amount of noise due to amplified spontaneous emission [31].

2.2. Realistic near-field source and critical coupling

In most cases, evanescent waves are created by illuminating an object with a propagating beam of a certain input power. The power not absorbed by the object, the imaging device, or the detector remains in the propagating beam or is scattered to other directions. If the imaging system consumes a small fraction of the input power, then the object can be regarded as an ideal current source, as described in the previous section. This assumption is sufficient for NSOM, as the probe can only extract a small fraction of input power. However, other near-field imaging systems, especially the ones based on the principle of resonance, may consume a significant portion of the input power, such that it is no longer valid to regard the object as a fixed current source.
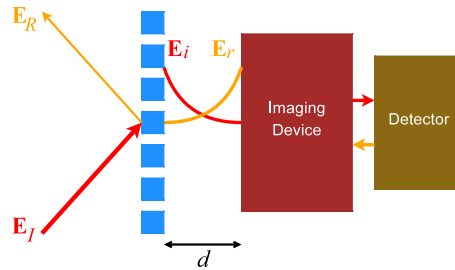

Fig. 3. A realistic near-field source that converts an input propagating wave $\mathbf{E}_I$ into an evanescent wave $\mathbf{E}_i$, to be detected by the imaging system, and a reflected wave $\mathbf{E}_R$ that carries unused power away from the source.

To model a more realistic near-field source, consider a generic object illuminated by an input wave denoted by $\mathbf{E}_I$. The object produces an evanescent wave $\mathbf{E}_i$ of a certain spatial frequency to be detected by the imaging system, as well as a reflected wave $\mathbf{E}_R$ that carries away any unused power, as shown in Fig. 3. The four waves are connected by the scattering matrix of the object:

$$\left(\begin{array}{c} \mathbf{E}_i \\ \mathbf{E}_R \end{array} \right) = \left(\begin{array}{cc} t & r' \\ r & t' \end{array} \right) \left(\begin{array}{c} \mathbf{E}_I \\ \mathbf{E}_r \end{array} \right). \tag{10}$$

We shall leave the nature of $\mathbf{E}_I$, $\mathbf{E}_R$, and the scattering matrix unspecified, so that $\mathbf{E}_I$ may be used to model any input power that supports the evanescent wave, and $\mathbf{E}_R$ may represent any form of unused power.

Let the scattering coefficients be scalars for simplicity, and consider the z component of the

tunneling Poynting vector:

$$S_z(0 < z < d) = \frac{\kappa}{\mu_0 \omega} \left| \frac{t\mathbf{E}_I}{1 - r'\Gamma \exp(-2\kappa d)} \right|^2 \mathrm{Im}\{\Gamma\} \exp(-2\kappa d). \tag{11}$$

If d is relatively large such that $\Gamma \exp(-2\kappa d)$ has a very small magnitude, the denominator of S_z, $|1 - r'\Gamma \exp(-2\kappa d)|^2$, can be approximated by 1. Then S_z is approximately given by

$$S_z \approx \frac{\kappa}{\mu_0 \omega} |t\mathbf{E}_I|^2 \mathrm{Im}\{\Gamma\} \exp(-2\kappa d). \tag{12}$$

which has the same form as the power supplied by a fixed current source given by Eq. (7). This justifies the assumption of a fixed current source when the dissipated power is relatively small. In this limit, the power increases when the system is closer to the object.

On the other hand, if $\Gamma \exp(-2\kappa d)$ has a large magnitude that dominates the denominator of S_z, S_z becomes

$$S_z \approx \frac{\kappa}{\mu_0 \omega} \left| \frac{t\mathbf{E}_I}{r'} \right|^2 \frac{\mathrm{Im}\{\Gamma\}}{|\Gamma|^2} \exp(2\kappa d). \tag{13}$$

In this limit, the power increases when the system is farther away from the object, analogous to the evanescent growth condition in a negative-index slab [2, 6]. It follows that, as long as the magnitude of $\Gamma \exp(-2\kappa d)$ is large enough, there must always be an optimal working distance d at which the power dissipated by the system is the largest. Such a condition is exactly the same as the critical coupling condition that occurs with resonators [14, 15, 16]. Undercoupling occurs when d is larger than the critical-coupling d, while overcoupling occurs when d is smaller.

To derive the optimal critical coupling condition, consider $\mathbf{E}_R$ in terms of $\mathbf{E}_I$:

$$\mathbf{E}_R = \frac{r + \Gamma(tt' - rr') \exp(-2\kappa d)}{1 - \Gamma r' \exp(-2\kappa d)} \mathbf{E}_I. \tag{14}$$

The reflected wave can be eliminated, and the power supplied to the imaging system becomes the largest, when

$$\Gamma \exp(-2\kappa d) = \frac{-r}{tt' - rr'}. \tag{15}$$

The response of the object, characterized by the right-hand side of Eq. (15), plays a significant role in determining when impedance matching is satisfied and critical coupling occurs.

The critical coupling condition depends crucially on the magnitude of $\Gamma \exp(-2\kappa d)$. To have a large working distance and still achieve critical coupling, it is important to have a high magnitude of Γ and thus high-quality resonance, in order to cancel the exponential decay factor $\exp(-2\kappa d)$.

3. Resonantly enhanced solid immersion microscopy (RESIM)

3.1. General principle

Another important problem in near-field imaging is how the evanescent waves can be detected in practice. For microscopy, one would like to convert evanescent waves into far-field radiation for easier detection. For lithography, on the other hand, it is desirable to shrink a far-field pattern into a near-field image with subwavelength features. Subwavelength far-field microscopy based on SPP resonance has been demonstrated by Smolyaninov *et al.* [20, 21], while a cylindrical metallic-dielectric structure with hyperbolic dispersion has also been proposed for microscopy

by Salandrino and Engheta [22] and Jacob *et al.* [23] and experimentally demonstrated by Liu *et al.* [24] and Smolyaninov *et al.* [25]. The signal power throughput is nonetheless hampered by the relatively high loss of metals, so the object has to be extremely close to the imaging device. The cylindrical geometry of the latter scheme is also inconvenient for lithography.
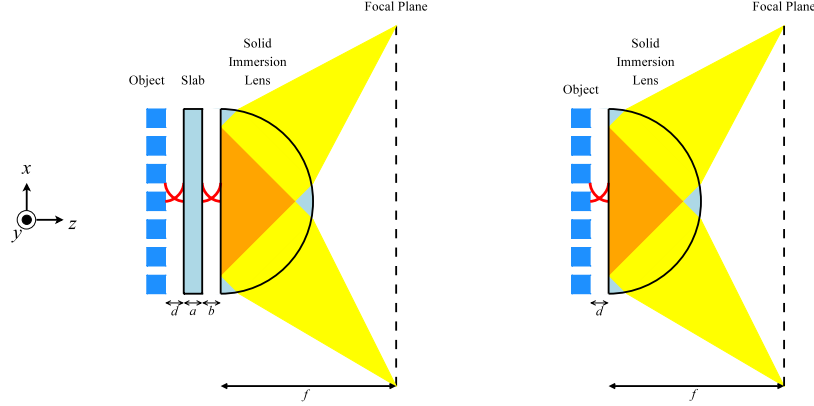

Fig. 4. Schematic of RESIM (left), compared with that of conventional solid immersion microscopy (right). The figures are not drawn to scale.

Since the resonantly enhanced waves in dielectric resonators are still propagation modes inside the dielectric, far-field optics techniques, such as lensing, can be used to convert the propagating waves inside a dielectric into propagating waves in free space. To efficiently retrieve near-field information in the far field, we hereby propose the method of resonantly enhanced solid immersion microscopy, or RESIM for short, schematically shown in Fig. 4. In RESIM, a dielectric planar resonator, such as a slab, is combined with a solid immersion lens [17] of the same refractive index to provide resonantly enhanced transmission of multiple spatial frequencies and both polarizations, while the solid immersion lens converts the evanescent waves into far-field radiation and projects the spatial spectrum onto the focal plane for detection. The system may also be used in reverse to convert far-field radiation at the focal plane to resonantly enhanced evanescent waves at the flat object plane for lithography.

3.2. Numerical example

To understand how the dielectric resonator helps the transmission of evanescent waves for solid immersion microscopy, assume for simplicity that the object is a fixed TE current line source,

$$\mathbf{J}(\mathbf{x}) = \hat{\mathbf{y}} I \delta(z) \delta(x), \tag{16}$$

and the image at the focal plane is the Fourier transform of the propagation waves inside the solid immersion lens without aberrations. The image at the focal plane can then be approximated by the transmitted electric field spectrum at $z = d + a + b$ inside the lens,

$$\mathbf{E}(z = d + a + b) = -\hat{\mathbf{y}} \frac{\mu_0 \omega I}{2} \frac{\tau(k_x)}{\sqrt{k^2 - k_x^2}}, \tag{17}$$

where $\tau(k_x)$ is the electric-field transmission coefficient across the multiple interfaces. For $\lambda = 230$ nm, a diamond thin film with $n = 2.7[1 + i/(2Q_i)]$, a material quality factor Q_i, and a thickness of $a = 500$ nm, and a diamond solid immersion lens [32] behind the slab, Fig. 5 plots the transmitted spatial frequency spectra $|\mathbf{E}(z = d + a + b)|^2$ for various parameters in

logarithmic scale, compared with that of a diamond solid immersion lens without the slab for the same working distance $d = 50$ nm. With the lens only, the exponential decay of evanescent waves in free space leads to greatly reduced transmission of high spatial frequencies. With a slab 50 nm in front of the lens, on the other hand, the transmission of specific spatial frequencies is resonantly enhanced by two orders of magnitude, even though the lens itself is now much farther away from the source.
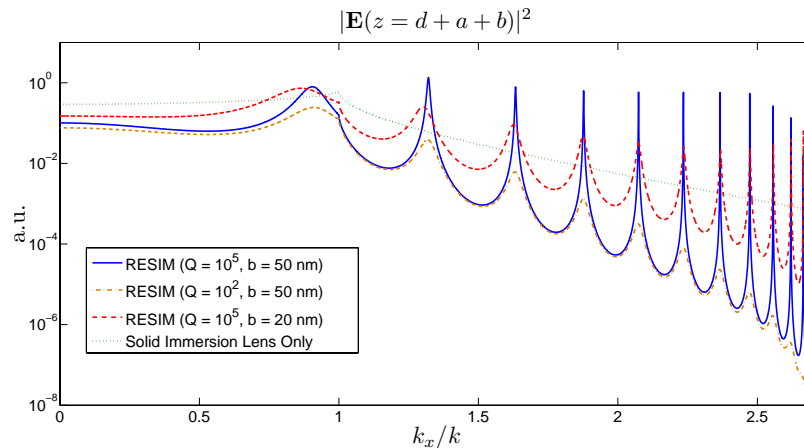
$$|\mathbf{E}(z = d + a + b)|^2$$

Fig. 5. Logarithmic plots of transmitted spatial frequency spectra of a RESIM device in front of a TE current line source for various parameters, compared with that of a solid immersion lens without the slab for the same working distance. Spatial frequency components with $k_x/k > 1$ are evanescent in free space. Other parameters are described in the text.

For a much lower Q_i of 10^2, although the spatial bandwidth of each resonance is broadened, the resonant enhancement is completely lost, due to severe dissipation in the slab. To control the trade-off between spatial bandwidth and resonant enhancement, it is better to damp the resonances by increasing the coupling between the slab and the lens. As shown in Fig. 5, if the $Q_i = 10^5$ slab is closer to the lens ($b = 20$ nm), one can increase the spatial bandwidth of each resonance while still maintaining some resonant enhancement.

3.3. Discussion

Resonant enhancement is necessarily accompanied by suppressed off-resonance transmission, as shown in Fig. 5, due to evanescent decay in the additional air gap. Still, the resonances can be used to raise the transmitted intensity at certain spatial frequencies above the noise floor of the detector at the focal plane, such that weaker signals can be detected, the working distance can be increased, and the signal-to-noise ratio can be improved for such spatial frequencies. The object can be digitally reconstructed using signal processing techniques [33], once the amplitude and phase of the discrete spatial frequency components are retrieved at the focal plane. Off-axis illumination or wavelength tuning may also be used to scan the spatial frequency spectrum of the object.

When using RESIM in reverse for lithography, only discrete spatial frequencies are resonantly enhanced in the near field at the object plane $z = 0$, but simple near-field pattern formation should still be possible by applying pattern formation techniques for conventional inteferometric lithography [34]. If the resonance mode with the highest spatial frequency is used for lithography of a sinusoidal pattern, the minimum achievable period, using the parameters given above, is approximately $\lambda/(2n) = 43$ nm, compared with the 120 nm period achieved in the

silver superlens experiment [8].

RESIM works with two-dimensional objects as well. Resonance modes exist in a dielectric slab as long as the transverse spatial frequency $(k_x^2 + k_y^2)^{1/2}$ satisfies the resonance condition, so the resonance modes are projected onto rings at the focal plane. The availability of such azimuthally degenerate modes in two dimensions provides more flexibility in near-field pattern formation for lithography. For example, an evanescent Bessel mode [35] can be formed with just one spatial frequency. A dielectric resonator also provides TM resonance modes that are nondegenerate with the TE modes.

In the preceding analysis, we have taken into account the multiple reflections across all interfaces, except the convex surface of the solid immersion lens and the object itself. An antireflection coating can conceivably be applied on the convex surface, such that parasitic reflection off this interface can be minimized. The response of the object may affect the resonance condition but should not affect the basic principles of resonant enhancement and lensing in RESIM.

We have also assumed that the finite transverse size of the slab and the lens in practice does not affect the operation of the proposed device. This assumption is valid as long as the transverse size L is much larger than the inverse bandwidth of each resonance, approximately given by $2\pi Q/k_x$. Otherwise a resonance mode would occupy a larger area than the finite slab, causing light to leak out from the side. The Q due to the finite size is therefore roughly given by

$$Q_s \sim \frac{k_x L}{2\pi} < \frac{nL}{\lambda}. \tag{18}$$

For $L = 1$ cm, $\lambda = 230$ nm, $n = 2.7$, nL/λ is 10^5, on the same order as Q_i.

If a small slab has to be used for practical reasons, a two-dimensional photonic bandgap structure [36] can be placed around the slab to prevent the leakage and improve the quality of resonances. The slab then effectively becomes a giant photonic bandgap defect. Notice that this use of photonic crystals is fundamentally different from photonic crystal imaging [10, 11], as the photonic bandgap effect does not play any direct role in the imaging process in our case and only provides confinement in the transverse dimension, so it is not necessary to fabricate a three-dimensional photonic crystal, which is a considerable challenge in practice.

4. Conclusion

In conclusion, high-quality resonance is desirable for optimal power transfer and working distance in near-field imaging. Low-loss dielectric resonators therefore have a distinct advantage over other proposed near-field imaging devices in this respect. The theoretical framework outlined in this paper may also be useful for other applications of photonic resonant enhancement, such as manipulation of nanoparticles [37] and wireless power supply [38, 39]. The strong resonant enhancement of dielectric structures may even be used to compensate for the inefficient generation of entangled photons in quantum lithography for further resolution enhancement [40, 41].

To illustrate the use of high-quality resonance for near-field imaging in practice, we have also proposed RESIM, the combination of a dielectric planar resonator with a solid immersion lens for resonantly enhanced near-field microscopy or lithography. The geometry is suitable for non-contact two-dimensional imaging or lithography and compatible with optofluidic technology [42], as well as other SPP or photonic crystal near-field imaging systems. We believe that the proposed device will find applications in nano-imaging, biological imaging, spectroscopy, lithography, and optical data storage.

The primary shortcoming of dielectric near-field imaging systems, compared with other proposed techniques, is the resolution limit imposed by the refractive index. For applications in

the near future, promising materials include silicon ($n = 3.5$, $\lambda = 1\ \mu$m, $\lambda/(2n) = 143$ nm), gallium phosphide ($n = 3.4$, $\lambda = 560$ nm, $\lambda/(2n) = 82$ nm) [43], potassium tantalate ($n = 2.5$, $\lambda = 350$ nm, $\lambda/(2n) = 70$ nm) [44], and diamond ($n = 2.7$, $\lambda = 230$ nm, $\lambda/(2n) = 43$ nm) [27, 28, 32]. To obtain an even higher refractive index, atomic resonance and coherence effects may be utilized to enhance the refractive index by an order of magnitude [45, 46]. The long-term success of dielectric near-field imaging will depend on the availability of transparent high-refractive-index materials.

Acknowledgments

A. Power dissipation for an aribitrary current distribution and an arbitrary photonic structure

For an arbitrary harmonic current distribution $\mathbf{J}(\mathbf{r})$ in free space, the electric field can be written in terms of $\mathbf{J}(\mathbf{r})$ and a tensoral Green's function,

$$\mathbf{E}_0(\mathbf{x}) = \int d^3\mathbf{x}' \overleftrightarrow{\mathbf{G}}(\mathbf{x} - \mathbf{x}') \cdot \mathbf{J}(\mathbf{x}'). \tag{19}$$

The Green's function can be separated into a far-field component and a near-field component,

$$\overleftrightarrow{\mathbf{G}} = \overleftrightarrow{\mathbf{G}}_f + \overleftrightarrow{\mathbf{G}}_n, \tag{20}$$

where the near-field component does not carry power by definition,

$$P_n = -\frac{1}{2} \int d^3\mathbf{x} \int d^3\mathbf{x}' \operatorname{Re}\left\{\mathbf{J}^*(\mathbf{x}) \cdot \overleftrightarrow{\mathbf{G}}_n(\mathbf{x} - \mathbf{x}') \cdot \mathbf{J}(\mathbf{x}')\right\} = 0. \tag{21}$$

If a photonic structure is present, the total electric field can be written, without loss of generality, as

$$\mathbf{E}(\mathbf{x}) = \mathbf{E}_0(\mathbf{x}) + \int d^3\mathbf{x}' \overleftrightarrow{\Gamma}(\mathbf{x}, \mathbf{x}') \cdot \mathbf{E}_0(\mathbf{x}'). \tag{22}$$

The total power supplied by the current source is

$$\begin{aligned} P = &-\frac{1}{2} \int d^3\mathbf{x} \int d^3\mathbf{x}' \operatorname{Re}\left\{\mathbf{J}^*(\mathbf{x}) \cdot \overleftrightarrow{\mathbf{G}}_f(\mathbf{x} - \mathbf{x}') \cdot \mathbf{J}(\mathbf{x}')\right\} \\ &-\frac{1}{2} \int d^3\mathbf{x} \int d^3\mathbf{x}' \int d^3\mathbf{x}'' \operatorname{Re}\left\{\mathbf{J}^*(\mathbf{x}) \cdot \overleftrightarrow{\Gamma}(\mathbf{x}, \mathbf{x}') \cdot \overleftrightarrow{\mathbf{G}}_f(\mathbf{x}' - \mathbf{x}'') \cdot \mathbf{J}(\mathbf{x}'')\right\} \\ &-\frac{1}{2} \int d^3\mathbf{x} \int d^3\mathbf{x}' \int d^3\mathbf{x}'' \operatorname{Re}\left\{\mathbf{J}^*(\mathbf{x}) \cdot \overleftrightarrow{\Gamma}(\mathbf{x}, \mathbf{x}') \cdot \overleftrightarrow{\mathbf{G}}_n(\mathbf{x}' - \mathbf{x}'') \cdot \mathbf{J}(\mathbf{x}'')\right\}. \end{aligned} \tag{23}$$

The first term on the right-hand side is the power of far-field radiation in free space, and the second term is the modification of the radiated power due to the reflected electric field. For example, the power radiated by the current source can be enhanced by putting the current source in a cavity, or inhibited by putting it in a photonic bandgap structure, where radiation is forbidden. The third term is the dissipated power due to the coupling of the near field to a dissipative load. For example, if a dielectric resonator is near the current source, power can be supplied into the resonance modes of the resonator. In this paper we are mainly concerned with the third term in a planar geometry.